

# Ultrastrong Terahertz Coupling in a van der Waals Heterostructure

F. Helmrich<sup>1</sup>, I. Khanonkin<sup>1</sup>, M. Kroner<sup>1</sup>, G. Scalari<sup>1</sup>, J. Faist<sup>1</sup>, A. İmamoğlu<sup>1</sup>, and T. F. Nova<sup>1</sup>

<sup>1</sup>Institute for Quantum Electronics, ETH Zürich, Auguste-Piccard-Hof 1, 8093 Zürich, Switzerland

## Abstract

The field of strongly coupled photon-matter systems aims to create novel hybrid phases that enhance or modify material properties. A key challenge has been developing versatile platforms for exploring cavity quantum electrodynamics (QED) of quantum materials. Here, we demonstrate and probe ultrastrong light-matter coupling in atomically-thin van der Waals materials. We developed a broadband time-domain microscope that integrates exfoliated, dual-gated, two-dimensional quantum materials with sub-wavelength photon confinement at terahertz frequencies. Using bilayer graphene as a model system, we perform spectroscopic studies across a wide range of frequencies and gate voltages. For the first time, we measure the field-tunable band gap of bilayer graphene at terahertz frequencies while simultaneously observing clear signatures of ultrastrong coupling, with interaction strengths exceeding  $\Omega/\omega \approx 40\%$ . Our work bridges the gap between theoretical predictions and experimental implementation of cavity QED in van der Waals materials, paving the way for further studies of exotic phases and novel light-matter states.

The control of quantum materials with light has emerged as an intriguing direction in materials science and condensed matter physics [1]. At the forefront of modern research is the vision that ground state properties of materials could be modified through interaction with cavity-confined electromagnetic fields [2]. Even in the absence of external stimuli, matter can couple to quantum fluctuations of the vacuum electromagnetic field, leading to the formation of hybrid light-matter states known as cavity polaritons [3]. In the regime of ultrastrong light-matter coupling, where the interaction strength becomes comparable to the energy of material excitations, these novel hybrid phases are predicted to exhibit strongly modified macroscopic

properties compared to the uncoupled system, with ground states that contain virtual light and matter excitations [4, 5]. Recent theoretical studies have proposed a range of fascinating phenomena in hybrid systems. These include the emergence of superconductivity due to electron-photon interactions [6], the potential for cavity-induced ferroelectric phase transitions [7, 8], as well as stabilization of superradiant excitonic insulators [9–12] and cavity-mediated control of intertwined orders [13]. These predictions highlight the transformative potential of strong light-matter coupling in quantum materials. Experiments have also shown impressive results demonstrating how confined electromagnetic fields can influence various systems. In the context of polariton chemistry [14], cavity-coupling to molecular vibrations has been shown to affect chemical reactivity [15–17]. In solid-state systems, the critical temperature in a metal-to-insulator transition has been controlled by suppressing the radiative heat flow to the material [18]. A recent study has demonstrated cavity-induced breakdown of topological protection at integer filling in the quantum Hall transport of two-dimensional (2D) electron gases [19]. However, especially in condensed matter systems, clear evidence of cavity coupling to quantum phases and modification of equilibrium properties due to vacuum fields remains scarce.

To address this gap, we have developed a platform specifically designed to explore the physics of strongly coupled light-matter quantum materials, with a particular emphasis on two-dimensional (2D) systems. Heterostructures of van der Waals materials serve as an excellent experimental framework, owing to their diverse array of quantum and correlated phases, ranging from superconductivity [20–27] and Wigner-Mott states [28–30] to exotic magnetism [31, 32]. Often, these phases can be explored within a single device by electrostatic gating, making van der Waals materials particularly versatile in the exploration of light-matter phases.

However, integrating 2D materials with suitable cavities presents significant challenges. Strong light-matter coupling occurs in the proximity of collective excitations, which for quantum materials lie within the terahertz photon range. Ultrastrong light-matter coupling in this frequency range is usually achieved by confining the electromagnetic field within a cavity mode noticeably smaller than the photon wavelength, which spans from tens to thousands of microns. While sub-wavelength localization of terahertz fields can be efficiently achieved using micro-structured metallic resonators, conventional approaches rely on metamaterials of

repeating resonators placed atop the material of interest [33]. This method is incompatible with exfoliated 2D materials, which are usually limited to in-plane dimensions of just a few microns.

Recent advancements have enabled spectroscopy of individual metallic resonators by adapting solid immersion lenses [34] to the terahertz range [35]. Building on this concept, we have developed a method that simultaneously achieves the broadband frequency operation necessary for quantum materials spectroscopy [36] and strong field confinement, while maintaining compatibility with gate-tunable van der Waals devices. Our approach addresses the limitations of conventional techniques in studying micro-structured devices, which often suffer from bandwidth constraints or incompatibility with dual gating. While on-chip terahertz techniques have proven highly effective in probing the ultra-low energy electrodynamics of 2D materials [37–41], they face inherent bandwidth limitations [42], typically not exceeding 1.5 THz or 6 meV. Notably, much of the physics of quantum [36] and van der Waals materials is expected or has been observed at energies of several to tens of meVs. This frequency range encompasses collective modes such as phonons [43], Mott gaps in Moiré systems [44], binding energies [45] as well as Higgs and Bardasis-Schrieffer modes in excitonic insulators [46, 47], and Wigner gap and excitations of Wigner crystals [48], among others. With a bandwidth exceeding 20 meV, our technique outperforms existing methods and bridges the gap between on-chip terahertz and photoconductivity measurements [44, 49, 50]. Importantly, our approach is versatile, being adaptable to various terahertz generation techniques and cavity designs. This flexibility makes it scalable across a wide range of frequency domains.

## Experimental Setup and Model System

In our setup (Fig. 1A), a free-space terahertz beam is tightly focused using a high-refractive-index, transparent hyper-hemispherical silicon lens. The beam impinges on a high-resistivity silicon substrate coated with gold, except for a small complementary bow-tie resonator designed to function for a broadband range of terahertz frequencies. This resonator steers the field onto a spot smaller than 2 microns, as represented by the antenna mode in Fig. 1C. The transmitted terahertz field (Fig.1B), with a bandwidth ranging from 1 to 6 THz (4 to 24 meV), is then recollimated by a secondary hemispherical silicon lens and detected using conventional far-field methods, such as electro-optic sampling within a nonlinear crystal. Crucially, only the

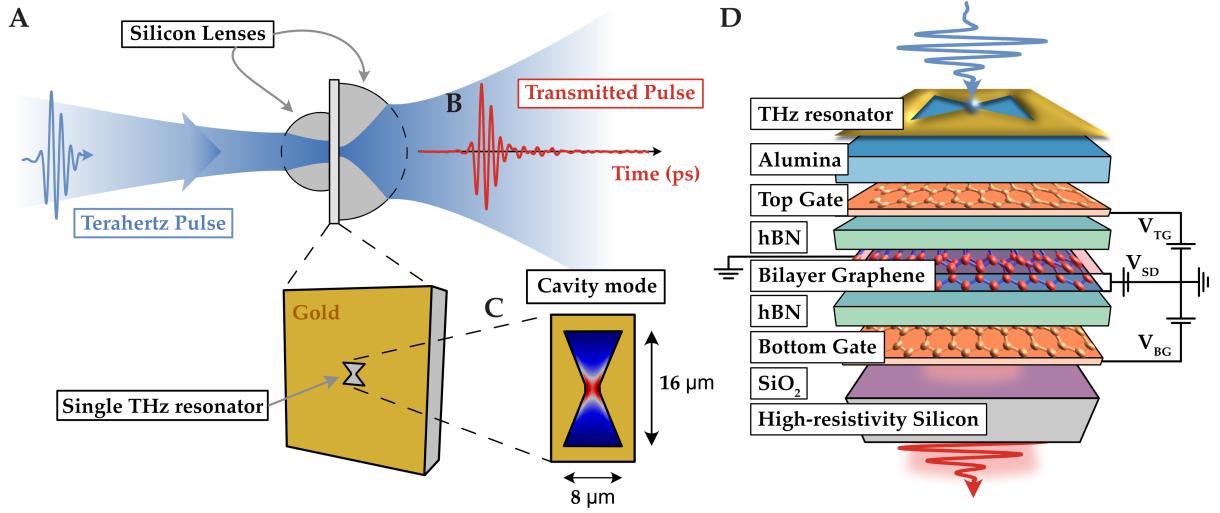


**Figure 1: Sub-wavelength terahertz spectroscopy of cavity-coupled bilayer graphene.** **A** A few-cycle terahertz pulse (blue line) is focused on a 2D heterostructure with a bow-tie resonator and solid immersion lenses. **B** Terahertz pulse transmitted through the immersion lenses and the resonator detected by electro-optic sampling. **C** In-plane electric field of the resonant cavity mode calculated with finite-element methods. The field is concentrated on the apex of the bow-tie. **D** Lateral view of the sample structure. The heterostructure consists of Bernal bilayer graphene, few-layer graphite gates and hBN dielectrics placed on a high-resistivity Si/SiO<sub>2</sub> substrate. The heterostructures is insulated from the bow-tie resonator with alumina dielectric.

field that traverses the micron-sized resonator focus is transmitted, enabling sub-wavelength, broadband terahertz spectroscopy of micron-sized samples positioned beneath the antenna focus (Fig. 1D).

We chose Bernal-stacked bilayer graphene (BLG) as our material system due to its ideal characteristics for studying light-matter interactions at their most extreme. While the material is intrinsically a semimetal with quasi-parabolic bands at the K and K' points, a unique “Mexican hat” band gap can be opened and controlled by application of a displacement field perpendicular to the graphene layers [51]. As a consequence, BLG offers strong optical excitations such as band-to-band transitions [52] and excitons [49] that can be continuously tuned from the mid-infrared to the terahertz range, perfectly aligning with our setup capabilities.

In our device (Fig. 1D), BLG is encapsulated between two hexagonal boron nitride (hBN) layers and is fully tunable with two thin graphite gates, allowing independent control of the charge density  $n = \frac{\epsilon_{\text{hBN}}\epsilon_0}{e} \left( \frac{V_{\text{TG}}}{d_{\text{TG}}} + \frac{V_{\text{BG}}}{d_{\text{BG}}} \right)$  and the out-of-plane displacement field  $D = \frac{\epsilon_{\text{hBN}}\epsilon_0}{2} \left( \frac{V_{\text{TG}}}{d_{\text{TG}}} - \frac{V_{\text{BG}}}{d_{\text{BG}}} \right)$ , where  $V_{\text{TG(BG)}}$ <sup>1</sup>,  $d_{\text{TG(BG)}}$ ,  $e$ ,  $\epsilon_{\text{hBN}}$ , and  $\epsilon_0$  are the top gate and bottom gate voltages, the hBN layer thicknesses, the elementary charge, the hBN dielectric constant ( $\approx 3.4$  [53]) and vac-

<sup>1</sup>Note that, for simplicity, we include the shift of charge neutrality from 0 V in the definition of  $V_{\text{BG}}$  and  $V_{\text{TG}}$ .

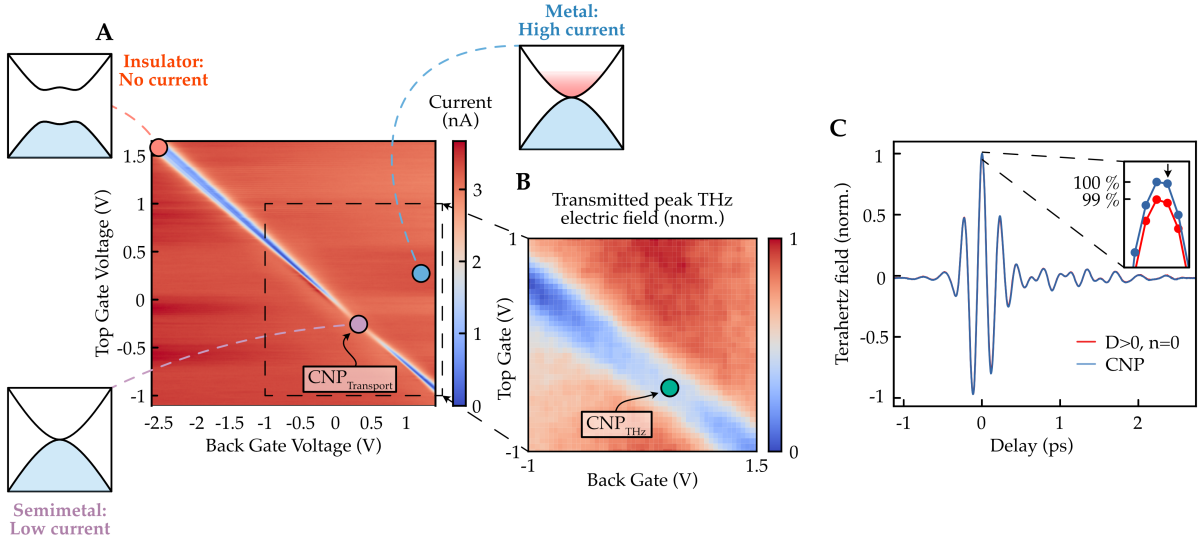


**Figure 2: Transport characteristics and terahertz transmission of the bilayer graphene device.** **A** BLG dual-gate conductivity measurement. The dots mark the CNP (purple), the insulating phase where the THz reference spectrum is recorded (orange,  $D = -0.35$  V/nm) and a representative metallic point (blue). **B** Terahertz field transmission at a fixed time delay, plotted against top and back gate voltages. The chosen time delay corresponds to the THz field maximum (indicated by the black arrow in panel C inset). The slightly shifted CNP extracted from the terahertz measurement is shown as a green dot. Data is normalized. **C** Transmitted terahertz pulses when BLG is at the CNP (blue) and in an insulating state with  $D > 0$  (red). The inset shows a closer view of the maximum of the waveforms. Both traces are normalized to the maximum of the blue curve. All measurements were taken at 5 K.

uum permittivity, respectively. Two Cr/Au etch contacts to BLG [54] allow us to probe the transport properties of the device. The stack is completed by the terahertz resonator, which is electrically insulated from the heterostructure and the electrical connections via a 140 nm layer of alumina grown by atomic layer deposition.

## Transport Characteristics and Terahertz Transmission

We first characterized the gate-voltage dependent two-point conductance of our device at 5 K (Fig. 2A), identifying the typical transport regimes of bilayer graphene. For  $V_{TG} = -V_{BG} \frac{d_{TG}}{d_{BG}}$ , the out-of-plane displacement field  $D$  breaks inversion symmetry between the two graphene layers, opening a band gap that results in a minimum in conductance typical of an insulating state. This line corresponds to the diagonal charge neutrality region in Fig. 2A, where  $n = 0$ . For  $V_{TG} = V_{BG} \frac{d_{TG}}{d_{BG}}$ , we increase the carrier concentration without opening a band gap, thus making the material metallic and increasing the conductivity. At the Charge Neutrality Point (CNP), where both  $n = 0$  and  $D = 0$ , the material behaves like a semimetal (purple dot in Fig. 2A).

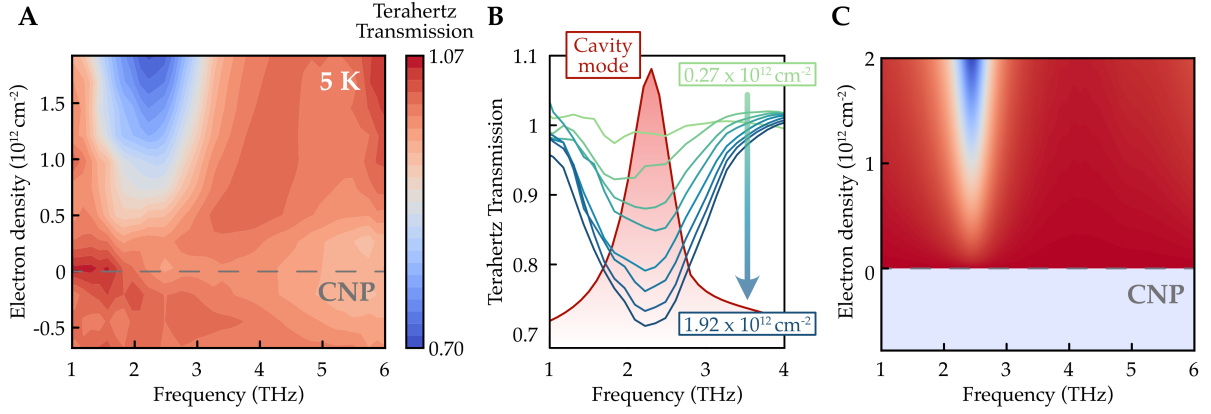


**Figure 3: Cavity modulation by doping.** **A** Contour plot of terahertz transmission spectra of BLG as a function of electron density  $n$  at zero displacement field ( $D = 0$ ). All spectra are normalized to the insulating state at  $D = -0.35$  V/nm. Measurements were taken at 5 K. **B** Line cuts of the spectra in panel A showing the dip in transmission. The red line represents the bare cavity transmission spectrum, calculated using finite-element methods. **C** Simulated transmission spectra of a linear cavity containing a Drude metal at its center, plotted as a function of electron density. All spectra are normalized to the bare cavity transmission spectrum.

In Fig. 2C, we show the terahertz pulse transmitted through the resonator, the stack and the silicon lenses when the device is biased at the CNP. For non-zero displacement ( $D \neq 0$ ) and zero carrier density ( $n = 0$ ), the opening of the band gap induces changes of a few percent in the terahertz amplitude (inset in Fig. 2C).

The gate-voltage dependence of the terahertz transmission at a fixed time delay (indicated by the black arrow in the Fig. 2C inset) is shown in Figure 2B. This transmission data bears a striking resemblance to the transport measurement results. A distinct charge neutrality line emerges, mirroring the insulating region observed in transport, with a nearly identical slope and intercept, albeit with a significantly larger width. Notably, the CNP location exhibits a slight shift along the charge neutrality line between the terahertz and transport measurements, as indicated by the purple and green dots in Figures 2A and 2B, respectively. We attribute this displacement to the probing of different sample locations in the two measurement types. Note that the single-time delay measurement does not provide spectral information. Nevertheless, the measurement in Fig. 2B clearly demonstrates that the terahertz signal is sensitive to the electronic state of BLG while remaining unaffected by other elements of the stack, including the gates.

## Doping-induced cavity mode screening

To gain insight into the optical properties of the coupled BLG/cavity system, we first measured the spectrally resolved terahertz transmission when BLG is doped. Fig. 3A shows the terahertz spectra measured for different charge densities with  $n \neq 0$  and  $D = 0$ . Each spectrum is referenced to the transmission taken for BLG in an insulating state ( $D = -0.35$  V/nm and  $n = 0$ ; red dot in Fig. 2A), where the band gap is larger than the terahertz bandwidth of our setup and the material becomes transparent for THz radiation. Effectively, the reference spectrum corresponds to the transmission of the bare cavity. It is crucial to note that changes in the normalized transmission spectra may originate from changes in either BLG or the cavity transmission properties. Here, we observe that for increasing electron densities, a pronounced dip in the terahertz transmission develops around 2.3 THz. The dip coincides with the peak position of the simulated cavity transmission spectrum (Fig. 3B), consistent with observations in ref. [55]. As the resonance frequency and linewidth remain unchanged (line cuts in Fig. 3B), we conclude that the primary effect is the screening of the cavity mode from the incoming field by the injected electrons, which results in reduced cavity transmission. The coupled system acts as a terahertz attenuator with modulation depths of around 30% in power for relatively small dopings. We qualitatively reproduce this behavior by simulating the interaction between a linear terahertz cavity and a material characterized by a Drude model with varying electron densities (Fig. 3C).

## Observation of ultrastrong Coupling and Polariton Formation

The transmission spectra as a function of displacement field  $D \neq 0$  for  $n = 0$  are shown in Figures 4A and B. At large negative fields, the material exhibits an insulating state with an electronic gap exceeding our detection window, resulting in a featureless response (pink curve at -0.33 V/nm in Fig. 4A). As the field decreases, an absorption edge emerges and shifts from higher to lower frequencies (dashed black line in Fig. 4A). This behavior is consistent with the field-tunable band gap of BLG, measured here for the first time in this frequency range. The calculated field dependence following the self-consistent Hartree model for screening of ref. [56] is shown in Figure 4B (dark blue line), in excellent agreement with the measured edge.

As the gap approaches the cavity frequency with further decreasing fields, the spectrum

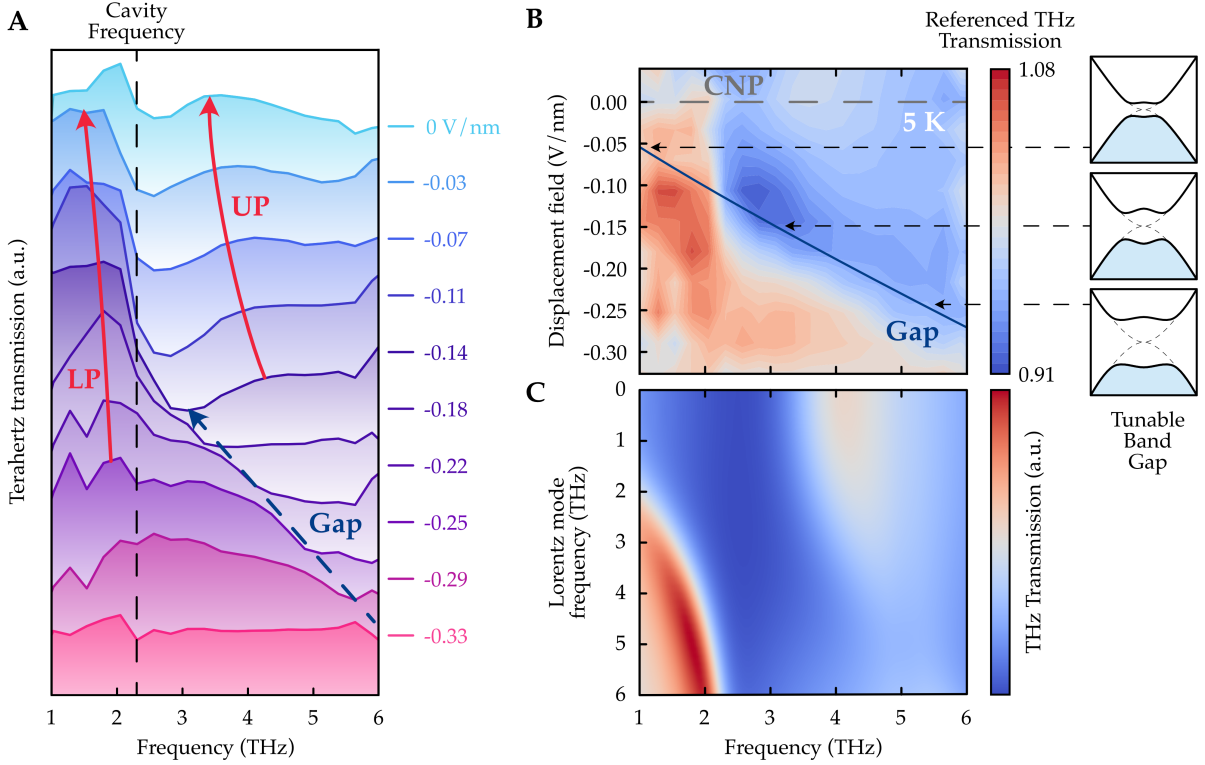


**Figure 4: Observation of ultrastrong coupling and polariton formation.** **A** BLG transmission spectra at various displacement fields ( $D$ ) under zero doping ( $n = 0$ ) measured at 5 K. All spectra are referenced to the insulating state at  $D = -0.35$  V/nm and vertically offset for clarity. The cavity resonance frequency is indicated by a dashed line. A black dashed arrow points to the closing band gap edge, while red arrows highlight the lower and upper polariton branches. **B** Contour plot representation of the spectra from panel A. The blue line represents the band gap calculated using the model from ref. [56], and the grey dashed line marks the CNP position. **C** Simulated transmission spectra of a linear cavity containing a Lorentz oscillator at its center, plotted as a function of oscillator frequency. All spectra are normalized to the bare cavity transmission spectrum.

undergoes dramatic changes. Two dispersive peaks develop: a strong, narrow peak below and a weak, broad peak above the cavity frequency. These modes correspond to the lower (LP) and upper (UP) polaritons, forming around a deepening polariton gap (the blue dip in Fig. 4B), characteristic of a strongly coupled light-matter system. The estimated coupling strength, defined by the ratio between the vacuum Rabi ( $\Omega$ ) and the cavity ( $\omega$ ) frequencies, is  $\eta = \Omega/\omega \approx 1 \text{ THz}/2.3 \text{ THz} = 43\%$ , which places our system well into the ultrastrong coupling regime ( $\eta > 10\%$  [4, 5]). The large coupling in our system aligns with the predictions of ref. [57]. We qualitatively capture these observations by simulating a linear terahertz cavity coupled to a material characterized by a Lorentz oscillator with a tunable resonance frequency. Importantly, the Lorentz model can be used even in the apparent absence of bound states [58]. This model effectively reproduces the key experimental findings: the formation of asymmetric polariton branches and the emergence of a gap in the terahertz spectrum (Fig. 4C).



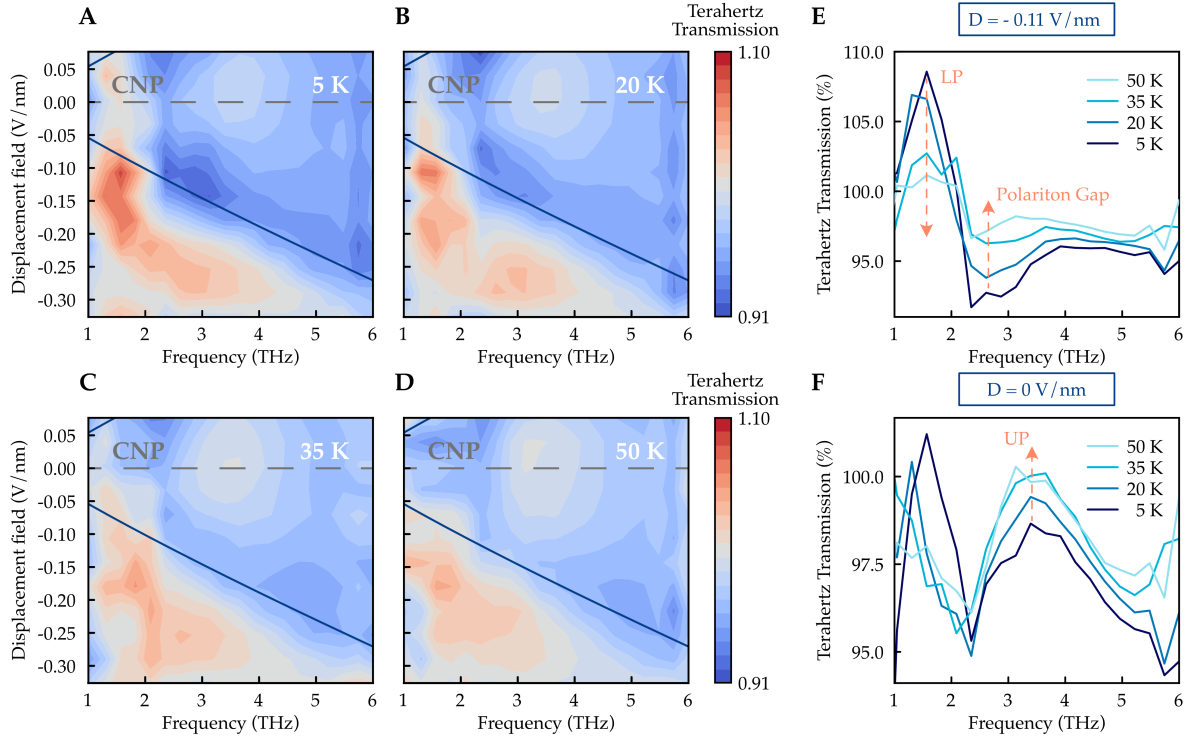


**Figure 5: Temperature dependence.** A-D Contour plots of the transmission spectra of BLG for different displacement fields  $D$  and zero doping ( $n = 0$ ) measured at 5 K (A), 20 K (B), 35 K (C) and 50 K (D). All spectra are referenced to the insulating state at  $D = -0.35$  V/nm. All spectra are normalized to the insulating phase obtained at  $D = -0.35$  V/nm. The calculated band gap is represented by a solid blue line, while a grey dashed line indicates the CNP. E, F Line cuts extracted from the spectra presented in panels A-D at  $D = 0.11$  V/nm (E) and at  $D = 0.00$  V/nm (F).

## Temperature Dependence

Figure 5 presents the temperature dependence of the polariton spectra at 5 K (A), 20 K (B), 35 K (C), and 50 K (D). As temperature increases, we observe a decrease in the contrast of all spectral features, with the lower polariton and the polariton gap weakening (Fig. 5E). Notably, the upper polariton strength increases with temperature (Fig. 5F). We attribute this behavior to non-radiative decay processes that become dominant at elevated temperatures, leading to line broadening. Interestingly, we do not observe a significant closing of the polariton gap at higher temperatures. This observation aligns with theoretical predictions that features of ultrastrong coupling persist even in the presence of strong dissipation [59].

## Conclusion

Our work demonstrates the successful integration of van der Waals materials with sub-wavelength terahertz cavities, achieving ultrastrong coupling with a remarkable strength of  $\approx 40\%$ . This accomplishment is twofold: first, it enables broadband terahertz spectroscopy of dual-gated and micron-sized materials, which was previously unobtainable with existing techniques. Second, it introduces a platform for creating ultrastrongly coupled light-matter quantum materials while taking advantage of the unique tunability and versatility of van der Waals heterostructures.

The observed coupling strength firmly places our system in the ultrastrong coupling regime, potentially leading to the realization of novel quantum phases and the ability to control material properties through cavity engineering. Future work could explore the impact of ultrastrong coupling on various quantum phenomena in van der Waals heterostructures, such as superconductivity, magnetism, and correlated states.

## References

- [1] A. de la Torre, D. M. Kennes, M. Claassen, S. Gerber, J. W. McIver, and M. A. Sentef. Colloquium: Nonthermal pathways to ultrafast control in quantum materials. *Rev. Mod. Phys.*, 93:041002, 2021.
- [2] F. Schlawin, D. M. Kennes, and M. A. Sentef. Cavity quantum materials. *Applied Physics Reviews*, 9(1):011312, 2022.
- [3] D. N. Basov, A. Asenjo-Garcia, P. J. Schuck, X. Zhu, and A. Rubio. Polariton panorama. *Nanophotonics*, 10(1):549–577, 2021.
- [4] A. Frisk Kockum, A. Miranowicz, S. De Liberato, S. Savasta, and F. Nori. Ultrastrong coupling between light and matter. *Nature Reviews Physics*, 1(1):19–40, 2019.
- [5] P. Forn-Díaz, L. Lamata, E. Rico, J. Kono, and E. Solano. Ultrastrong coupling regimes of light-matter interaction. *Rev. Mod. Phys.*, 91:025005, 2019.

- [6] F. Schlawin, A. Cavalleri, and D. Jaksch. Cavity-Mediated Electron-Photon Superconductivity. *Phys. Rev. Lett.*, 122:133602, 2019.
- [7] Y. Ashida, A. İmamoğlu, J. Faist, D. Jaksch, A. Cavalleri, and E. Demler. Quantum Electrodynamical Control of Matter: Cavity-Enhanced Ferroelectric Phase Transition. *Phys. Rev. X*, 10:041027, 2020.
- [8] S. Latini, D. Shin, S. A. Sato, Ch. Schäfer, U. De Giovannini, H. Hübener, and A. Rubio. The ferroelectric photo ground state of SrTiO<sub>3</sub>: Cavity materials engineering. *Proceedings of the National Academy of Sciences*, 118(31):e2105618118, 2021.
- [9] D. De Bernardis, T. Jaako, and P. Rabl. Cavity quantum electrodynamics in the nonperturbative regime. *Phys. Rev. A*, 97:043820, 2018.
- [10] G. Mazza and A. Georges. Superradiant quantum materials. *Phys. Rev. Lett.*, 122:017401, 2019.
- [11] G. M. Andolina, F. M. D. Pellegrino, V. Giovannetti, A. H. MacDonald, and M. Polini. Cavity quantum electrodynamics of strongly correlated electron systems: A no-go theorem for photon condensation. *Phys. Rev. B*, 100:121109, 2019.
- [12] G. M. Andolina, F. M. D. Pellegrino, V. Giovannetti, A. H. MacDonald, and M. Polini. Theory of photon condensation in a spatially varying electromagnetic field. *Phys. Rev. B*, 102:125137, 2020.
- [13] J. Li and M. Eckstein. Manipulating Intertwined Orders in Solids with Quantum Light. *Phys. Rev. Lett.*, 125:217402, 2020.
- [14] F. J. Garcia-Vidal, C. Ciuti, and Th. W. Ebbesen. Manipulating matter by strong coupling to vacuum fields. *Science*, 373(6551):eabd0336, 2021.
- [15] A. Thomas, J. George, A. Shalabney, M. Dryzhakov, S. J. Varma, J. Moran, T. Chervy, X. Zhong, E. Devaux, C. Genet, J. A. Hutchison, and Th. W. Ebbesen. Ground-State Chemical Reactivity under Vibrational Coupling to the Vacuum Electromagnetic Field. *Angewandte Chemie International Edition*, 55(38):11462–11466, 2016.
- [16] A. Thomas, L. Lethuillier-Karl, K. Nagarajan, R. M. A. Vergauwe, J. George, T. Chervy, A. Shalabney, E. Devaux, C. Genet, J. Moran, and Th. W. Ebbesen. Tilting a ground-state reactivity landscape by vibrational strong coupling. *Science*, 363(6427):615–619, 2019.

- [17] W. Ahn, J. F. Triana, F. Recabal, F. Herrera, and B. S. Simpkins. Modification of ground-state chemical reactivity via light–matter coherence in infrared cavities. *Science*, 380(6650):1165–1168, 2023.
- [18] G. Jarc, S. Y. Mathengattil, A. Montanaro, F. Giusti, E. M. Rigoni, R. Sergo, F. Fassiolli, S. Winnerl, S. Dal Zilio, D. Mihailovic, P. Prelovšek, M. Eckstein, and D. Fausti. Cavity-mediated thermal control of metal-to-insulator transition in  $1T\text{-TaS}_2$ . *Nature*, 622(7983):487–492, 2023.
- [19] F. Appugliese, J. Enkner, G. L. Paravicini-Bagliani, M. Beck, Ch., W. Wegscheider, G. Scalari, C. Ciuti, and J. Faist. Breakdown of topological protection by cavity vacuum fields in the integer quantum Hall effect. *Science*, 375(6584):1030–1034, 2022.
- [20] Y. Cao, V. Fatemi, S. Fang, K. Watanabe, T. Taniguchi, E. Kaxiras, and P. Jarillo-Herrero. Unconventional superconductivity in magic-angle graphene superlattices. *Nature*, 556(7699):43–50, 2018.
- [21] H. Zhou, T. Xie, T. Taniguchi, K. Watanabe, and A. F. Young. Superconductivity in rhombohedral trilayer graphene. *Nature*, 598(7881):434–438, 2021.
- [22] H. Zhou, L. Holleis, Y. Saito, L. Cohen, W. Huynh, C. L. Patterson, F. Yang, T. Taniguchi, K. Watanabe, and A. F. Young. Isospin magnetism and spin-polarized superconductivity in Bernal bilayer graphene. *Science*, 375(6582):774–778, 2022.
- [23] Y. Zhang, R. Polski, A. Thomson, É. Lantagne-Hurtubise, C. Lewandowski, H. Zhou, K. Watanabe, T. Taniguchi, J. Alicea, and S. Nadj-Perge. Enhanced superconductivity in spin–orbit proximitized bilayer graphene. *Nature*, 613(7943):268–273, 2023.
- [24] C. Li, F. Xu, J. Li, B. and Li, G. Li, K. Watanabe, T. Taniguchi, B. Tong, L. Shen, J. and Lu, J. Jia, F. Wu, X. Liu, and T. Li. Tunable superconductivity in electron- and hole-doped Bernal bilayer graphene. *Nature*, 631(8020):300–306, 2024.
- [25] Y. Guo, J. Pack, J. Swann, L. Holtzman, M. Cothrine, K. Watanabe, T. Taniguchi, D. Mandrus, K. Barmak, J. Hone, A. J. Millis, A. N. Pasupathy, and C. R. Dean. Superconductivity in twisted bilayer  $\text{WSe}_2$ . arxiv:2406.03418, 2024.
- [26] Y. Xia, Z. Han, K. Watanabe, T. Taniguchi, J. Shan, and K. F. Mak. Unconventional superconductivity in twisted bilayer  $\text{WSe}_2$ . arxiv:2405.14784, 2024.

- [27] L. Holleis, C. L. Patterson, Y. Zhang, Y. Vituri, H. Mo Yoo, H. Zhou, T. Taniguchi, K. Watanabe, E. Berg, S. Nadj-Perge, and A. F. Young. Nematicity and Orbital Depairing in Superconducting Bernal Bilayer Graphene with Strong Spin Orbit Coupling. arxiv:2303.00742, 2024.
- [28] Y. Shimazaki, I. Schwartz, K. Watanabe, T. Taniguchi, M. Kroner, and A. Imamoğlu. Strongly correlated electrons and hybrid excitons in a moiré heterostructure. *Nature*, 580(7804):472–477, 2020.
- [29] E. C. Regan, D. Wang, C. Jin, M. I. Bakti Utama, B. Gao, X. Wei, S. Zhao, W. Zhao, Z. Zhang, K. Yumigeta, M. Blei, J.D. Carlström, K. Watanabe, T. Taniguchi, S. Tongay, M. Crommie, A. Zettl, and F. Wang. Mott and generalized Wigner crystal states in WSe<sub>2</sub>/WS<sub>2</sub> moiré superlattices. *Nature*, 579(7799):359–363, 2020.
- [30] Y. Tang, L. Li, T. Li, Y. Xu, S. Liu, K. Barmak, K. Watanabe, T. Taniguchi, A. H. MacDonald, J. Shan, and K. F. Mak. Simulation of Hubbard model physics in WSe<sub>2</sub>/WS<sub>2</sub> moiré superlattices. *Nature*, 579(7799):353–358, 2020.
- [31] L. Ciorciaro, T. Smoleński, N. Morera, I. and Kiper, S. Hiestand, M. Kroner, Y. Zhang, K. Watanabe, T. Taniguchi, E. Demler, and A. Imamoğlu. Kinetic magnetism in triangular moiré materials. *Nature*, 623(7987):509–513, 2023.
- [32] Z. Tao, W. Zhao, B. Shen, T. Li, P. Knüppel, K. Watanabe, T. Taniguchi, J. Shan, and K. F. Mak. Observation of spin polarons in a frustrated moiré hubbard system. *Nature Physics*, 20(5):783–787, 2024.
- [33] G. Scalari, C. Maissen, D. Turčinková, D. Hagenmüller, S. De Liberato, C. Ciuti, C. Reichl, D. Schuh, W. Wegscheider, M. Beck, and J. Faist. Ultrastrong Coupling of the Cyclotron Transition of a 2D Electron Gas to a THz Metamaterial. *Science*, 335(6074):1323–1326, 2012.
- [34] A. N. Vamivakas, M. Atatüre, J. Dreiser, S. T. Yilmaz, A. Badolato, A. K. Swan, B. B. Goldberg, A. Imamoğlu, and M. S. Ünlü. Strong extinction of a far-field laser beam by a single quantum dot. *Nano Letters*, 7(9):2892–2896, 2007.
- [35] S. Rajabali, S. Markmann, E. Jöchl, M. Beck, C. A. Lehner, W. Wegscheider, J. Faist, and G. Scalari. An ultrastrongly coupled single terahertz meta-atom. *Nature Communications*, 13(1):2528, 2022.

- [36] D. N. Basov, R. D. Averitt, D. van der Marel, M. Dressel, and K. Haule. Electrodynamics of correlated electron materials. *Rev. Mod. Phys.*, 83:471–541, 2011.
- [37] P. Gallagher, C.-S. Yang, T. Lyu, F. Tian, R. Kou, H. Zhang, K. Watanabe, T. Taniguchi, and F. Wang. Quantum-critical conductivity of the Dirac fluid in graphene. *Science*, 364(6436):158–162, 2019.
- [38] J. W. McIver, B. Schulte, F.-U. Stein, T. Matsuyama, G. Jotzu, G. Meier, and A. Cavalleri. Light-induced anomalous Hall effect in graphene. *Nature Physics*, 16(1):38–41, 2020.
- [39] A. M. Potts, A. K. Nayak, M. Nagel, K. Kaj, B. Stamenic, D. D. John, R. D. Averitt, and A. F. Young. On-Chip Time-Domain Terahertz Spectroscopy of Superconducting Films below the Diffraction Limit. *Nano Letters*, 23(9):3835–3841, 2023. PMID: 37126575.
- [40] W. Zhao, S. Wang, S. Chen, Z. Zhang, K. Watanabe, T. Taniguchi, A. Zettl, and F. Wang. Observation of hydrodynamic plasmons and energy waves in graphene. *Nature*, 614(7949):688–693, 2023.
- [41] G. Kipp, H. M. Bretscher, B. Schulte, D. Herrmann, K. Kusyak, M. W. Day, S. Kesavan, T. Matsuyama, X. Li, S. M. Langner, J. Hagelstein, F. Sturm, A. M. Potts, Ch. J. Eckhardt, Y. Huang, K. Watanabe, T. Taniguchi, A. Rubio, D. M. Kennes, M. A. Sentef, E. Baudin, G. Meier, M. H. Michael, and J. W. McIver. Cavity electrodynamics of van der Waals heterostructures. arxiv:2403.19745, 2024.
- [42] D.R. Grischkowsky. Optoelectronic characterization of transmission lines and waveguides by terahertz time-domain spectroscopy. *IEEE Journal of Selected Topics in Quantum Electronics*, 6(6):1122–1135, 2000.
- [43] S. Hastrup, M. Strange, M. Pandey, Th. Deilmann, P. S. Schmidt, N. F. Hinsche, M. N. Gjerding, D. Torelli, P. M. Larsen, A. C. Riis-Jensen, J. Gath, K. W. Jacobsen, J. J. Mortensen, Th. Olsen, and K. S. Thygesen. The Computational 2D Materials Database: high-throughput modeling and discovery of atomically thin crystals. *2D Materials*, 5(4):042002, sep 2018.
- [44] J. Yang, G. Chen, T. Han, Q. Zhang, Y.-H. Zhang, L. Jiang, B. Lyu, H. Li, K. Watanabe, T. Taniguchi, Z. Shi, T. Senthil, Y. Zhang, F. Wang, and L. Ju. Spectroscopy sig-

- natures of electron correlations in a trilayer graphene/hbn moiré superlattice. *Science*, 375(6586):1295–1299, 2022.
- [45] L. Ma, P. X. Nguyen, Z. Wang, Y. Zeng, K. Watanabe, T. Taniguchi, A. H. MacDonald, K. F. Mak, and J. Shan. Strongly correlated excitonic insulator in atomic double layers. *Nature*, 598(7882):585–589, Oct 2021.
- [46] Z. Sun and A. J. Millis. Bardasis-Schrieffer polaritons in excitonic insulators. *Phys. Rev. B*, 102:041110, 2020.
- [47] Fei Xue, Fengcheng Wu, and A. H. MacDonald. Higgs-like modes in two-dimensional spatially indirect exciton condensates. *Phys. Rev. B*, 102:075136, 2020.
- [48] S. Brem and E. Malic. Terahertz Fingerprint of Monolayer Wigner Crystals. *Nano Letters*, 22(3):1311–1315, 2022. PMID: 35048702.
- [49] L. Ju, L. Wang, T. Cao, T. Taniguchi, K. Watanabe, S. G. Louie, F. Rana, J. Park, J. Hone, F. Wang, and P. L. McEuen. Tunable excitons in bilayer graphene. *Science*, 358(6365):907–910, 2017.
- [50] Q. Ma, R. Krishna Kumar, S.-Y. Xu, F. H. L. Koppens, and J. C. W. Song. Photocurrent as a multiphysics diagnostic of quantum materials. *Nature Reviews Physics*, 5(3):170–184, 2023.
- [51] E. McCann and M. Koshino. The electronic properties of bilayer graphene. *Reports on Progress in Physics*, 76(5):056503, 2013.
- [52] Y. Zhang, T.-T. Tang, C. Girit, Z. Hao, M. C. Martin, A. Zettl, M. F. Crommie, Y. R. Shen, and F. Wang. Direct observation of a widely tunable bandgap in bilayer graphene. *Nature*, 459(7248):820–823, 2009.
- [53] A. Pierret, D. Mele, H. Graef, J. Palomo, T. Taniguchi, K. Watanabe, Y. Li, B. Toury, C. Journet, P. Steyer, V. Garnier, A. Loiseau, J.-M. Berroir, E. Bocquillon, G. Fève, C. Voisin, E. Baudin, M. Rosticher, and B. Plaçais. Dielectric permittivity, conductivity and breakdown field of hexagonal boron nitride. *Materials Research Express*, 9(6):065901, jun 2022.
- [54] L. Wang, I. Meric, P. Y. Huang, Q. Gao, Y. Gao, H. Tran, T. Taniguchi, K. Watanabe, L. M. Campos, D. A. Muller, J. Guo, P. Kim, J. Hone, K. L. Shepard, and C. R. Dean. One-dimensional electrical contact to a two-dimensional material. *Science*, 342(6158):614–617, 2013.

- [55] F. Valmorra, G. Scalari, C. Maissen, W. Fu, Ch. Schönenberger, J. W. Choi, H. G. Park, M. Beck, and J. Faist. Low-Bias Active Control of Terahertz Waves by Coupling Large-Area CVD Graphene to a Terahertz Metamaterial. *Nano Letters*, 13(7):3193–3198, 2013.
- [56] E. McCann. Asymmetry gap in the electronic band structure of bilayer graphene. *Phys. Rev. B*, 74:161403, 2006.
- [57] S. De Liberato. Perspectives for gapped bilayer graphene polaritonics. *Phys. Rev. B*, 92:125433, 2015.
- [58] J. Khurgin. Excitonic radius in the cavity polariton in the regime of very strong coupling. *Solid State Communications*, 117:307–310, 01 2001.
- [59] S. De Liberato. Virtual photons in the ground state of a dissipative system. *Nature Communications*, 8(1):1465, 2017.